



# Quantitative analysis of organosulphur compounds in crude oil samples using magnetic solid phase extraction based on Au-Fe<sub>3</sub>O<sub>4</sub> adsorbent and gas chromatography with time-of-flight mass spectrometry

Samuel S. Mgiba<sup>1,2</sup> · V. Mhuka<sup>1</sup> · N. C. Hintsho-Mbita<sup>3</sup> · Nomvano Mketo<sup>1</sup>

Received: 23 September 2023 / Accepted: 13 April 2024  
© The Author(s) 2024

## Abstract

This study focused on the development of a magnetic solid phase extraction (m-SPE) method using Au-Fe<sub>3</sub>O<sub>4</sub> as an adsorbent followed by GC-ToFMS analysis for the determination of organosulphur compounds (OSCs) in fuel samples. The m-SPE using Au-Fe<sub>3</sub>O<sub>4</sub> NPs was preferred because of the low toxicity of the adsorbent<sup>1</sup>, high separation efficiency using external magnet<sup>2</sup> and greater extraction selectivity between sulphur and Au atom<sup>3</sup>. The Au-Fe<sub>3</sub>O<sub>4</sub> NPs were characterized using XRD, UV-Vis, TEM, SEM and FTIR. This method was optimized using multivariate analysis based on a two-level full factorial and central composite designs. The conditions which produced optimum efficiency were found to be 150 mg mass of sorbent, 100 µL eluent volume, 50 min extraction time and 6,5 pH of the sample. These optimum conditions showed a relatively low limit of detection in the range of 0.02–0.199 µg/g and limit of quantification of 0.08–0.602 µg/g. Furthermore, a relative standard deviation of triplicates analysis was between 0.8 and 2.3% with good linearity of 0.9816–0.9961. The percentage recovery for thiophene, 3-methylthiophene, benzothiophene and dibenzothiophene ranged from 76 to 95% for the spiked samples. The optimized m-SPE method was then applied in real fuel oil samples. The concentration of thiophene, 3-methylthiophene, benzothiophene and dibenzothiophene in crude oil, gasoline, diesel and kerosene ranged from 0.43–1.94 µg/g, 0.78–1.63 µg/g, 0.95–4.31 µg/g to 1.55–2.09 µg/g, respectively. The m-SPE, followed by GC-ToFMS method, proved to be efficient, inexpensive and an alternative method for OSCs analysis in fuel oils.

**Keywords** Magnetic solid phase extraction · Au-Fe<sub>3</sub>O<sub>4</sub> adsorbent · Organosulphur compounds · GC-ToFMS · Gasoline · Diesel · Kerosene

## Introduction

Crude oil is a mixture of hydrocarbons, heteroatoms and metals, with sulphur being the most abundant heteroatom. The maturity of crude oil is confirmed by the presence of polycyclic aromatic sulphur heterocyclic compounds (PASHs) (Garcia et al. 2021; Liu et al. 2010). The identification and quantification of organosulphur compounds (OSCs) in crude oil is challenging due to their molecular size and substituent structure. Chromatographic techniques were employed for crude oil analysis due to the complexity of crude oil and low concentration levels of OSCs (Anderson et al. 2006; Khalilian and Rezaee 2014). To minimize these challenges, sample pre-treatment methods have been developed (Mgiba et al. 2021).

✉ Nomvano Mketo  
nomvano.mketo@gmail.com; mketon@unisa.ac.za

<sup>1</sup> Department of Chemistry, College of Science, Engineering and Technology (CSET), University of South Africa, Florida Science Campus, Johannesburg 1709, South Africa

<sup>2</sup> Department of Maths, Science and Technology Education, Faculty of Humanities, University of Limpopo, Polokwane 0727, South Africa

<sup>3</sup> Department of Chemistry, Faculty of Science and Agriculture, University of Limpopo, Polokwane 0727, South Africa

One widely applied sample pre-treatment method is solid phase extraction (SPE), which is used for clean-up, pre-concentration and target analyte isolation (Patel et al. 2019). This technique was applied to analyse OSCs in petroleum asphalt (da Silveira et al. 2017) and sea crude oils (Yang et al. 2013). Another method is head space solid phase extraction (HSSE), which is an extension of stir bar sorptive extraction (SBSE). This method was previously used to identify two OSC compounds not reported previously in beer, 3-methylthiophene and 2-methyl-1-butanethiol (Hill and Smith 2000). The HSSE method showed the highest adsorption capacity and yielded an RSD range of 4.5–10.2% and a limit of detection of 0.04–10.48  $\mu\text{g L}^{-1}$  when using sol gel carbowax as sorptive bar for organosulphur compound analysis in water (Yu et al. 2008).

Magnetic solid phase extraction (mSPE) is a popular method for analysing complex samples due to its simplicity, environmental friendliness and high efficiency. It involves adding a magnetic sorbent to an aqueous sample, separated by an external magnet field, and elution (Manousi et al. 2021). Magnetic nanoparticles, such as magnetite, are popular due to their low price and low toxicity. However, magnetite lacks selectivity for complex samples, so it needs to be functionalized and modified (Heidari and Razmi 2012). Various materials, such as polymers (Biehl and Schacher 2020), silica (Šulek et al. 2010), carbon (Zhao et al. 2015), gold (Ghorbani et al. 2015) and metal oxides (Tan et al. 2015), can be used to modify magnetite. This study aims to synthesize supported gold-coated magnetite nanoparticles for mSPE, using the second-level full factorial design as a screening method and central composite design as a response surface methodology for optimization of significant parameters. Gold was chosen to coat the magnetite due to its ability to bind thiolated compounds on its surface because of the  $\pi$ -electron conjugation between the thiol groups and the gold atom (Lau et al. 2023).

## Experimental

### Materials and standards

The following salts iron (III)Chloride hexahydrate ( $\text{FeCl}_3 \cdot 6\text{H}_2\text{O}$ ) ACS reagent, ferrous chloride tetrahydrate ( $\text{FeCl}_2 \cdot 4\text{H}_2\text{O}$ ), sodium citrate dihydrate  $\geq 99\%$  FG [ $\text{HOC}(\text{COONa})(\text{CH}_2\text{COONa})_2 \cdot 2\text{H}_2\text{O}$ ], tetrachloroauric acid ( $\text{HAuCl}_4 \cdot 3\text{H}_2\text{O}$ )  $\sim 49\%$  Au, sodium hydroxide (NaOH) and acetonitrile (99.8%) were purchased from Sigma-Aldrich (Johannesburg, South Africa). Organosulphur standards, dibenzothiophene (98%), 3-methylthiophene (98%), thiophene ( $\geq 99\%$ ), benzothiophene (95%) and benzo[b] naphtha[1,2-d]thiophene were also purchased from Sigma-Aldrich (Johannesburg, South Africa). The

standards were dissolved in dichloromethane to form 1000 ppm stock solutions. Different solutions including 28 w/v % ammonium solution, hydrochloric acid (98%) were also purchased from Sigma-Aldrich (Johannesburg, South Africa). Diesel, petroleum and paraffin samples were purchased from a local filling station (South Africa, Johannesburg). Nitric acid (65%), hydrochloric acid (37%) was supplied by Merck (South Africa). Ultrapure water which was used during the project with resistivity of 18.2  $\text{M}\Omega \cdot \text{cm}$  was obtained from a Milli-Q system.

## Instrumentation

### Gas chromatography

The samples were analysed using a LECO Pegasus High Throughput (HT) gas chromatographic time-of-flight mass spectrometry (GC-ToF-MS) system equipped with Agilent GC model 7890 (Agilent Technology, Santa Clara, California, USA) used for quantitative analysis of OSCs. A Gerstel MPS2 Liquid/HS/SPME auto-sampler was used for loading the samples to be analysed. Injection of 1  $\mu\text{L}$  of the samples was performed using a split/splitless injector set at 300 °C. An HP-5 m J&W capillary column with the dimension of 30 m  $\times$  0.25 mm  $\times$  0.25  $\mu\text{m}$  film thickness with 5%- diphenyl/95% -dimethyl polysiloxane stationary phase was used for separation. Data acquisition was done using Leco chromaTOF software. The oven conditions used for separation were as follows: The initial temperature was set at 50 °C for a duration of 2 min until 140 °C. It was then ramped at 20 °C/min until 200 °C for 2 min. The ramping rate was increased to 30.00 °C/min and kept constant for 5 min until 260 °C.

A carrier gas Helium (99.999%, Afrox, Johannesburg, South Africa) was used under constant flow of 1  $\text{mL min}^{-1}$ . The GC/ToFMS interface temperature was set at 250 °C, and mass spectra were obtained at 70 eV in full scan mode (scanning  $m/z$  ranging from 45 to 450). Data were analysed using ChromaToF-HRT software.

### Ultraviolet-visible spectrometry

The Genesys 180 UV-Visible spectrophotometer was used for confirmation of the nanoparticles of  $\text{Fe}_3\text{O}_4$  and  $\text{Au-Fe}_3\text{O}_4$ . The dissolved solid samples ( $\text{Fe}_3\text{O}_4$  and  $\text{Au-Fe}_3\text{O}_4$ ) were first put in centrifuge tubes and diluted to make it less concentrated. Blank samples references were also prepared prior to analysis of real samples using distilled water. The samples were then run with wavelength range of 200–1200 nm.

### Scanning electron microscope (SEM–EDX)

The morphology of the nanoparticles was confirmed used SEM–EDX. The scanning electron microscope (SEM) measurements were taken on a Tescan Vega 3 LMH at a voltage of 20 kV, with a secondary electron detector (SED) and energy-dispersive X-ray spectroscopy (EDX). Prior to measurement, the samples were carbon-coated with the Agar Turbo Carbon coater to improve their conductivity.

### Fourier transform infrared spectroscopy (FT–IR)

The functional groups of the nanoparticles and its structural changes were investigated using the Fourier transformed infrared (FTIR) spectra with a Bruker Tensor 27 FTIR spectrophotometer. The synthesized samples were mixed with potassium bromide (KBr) before being compressed into pellets. During the analysis, data were collected from 400 to 4000  $\text{cm}^{-1}$  region.

### X-ray powder diffraction (XRD)

The crystal structure of the nanoparticles was determined using the X-ray diffraction (XRD). XRD measurements were taken with a PANalytical X'Pert Pro powder diffractometer. It was fitted with a 1D X'Celerator detector, upper levels of 6.67 and 12.78 keV, respectively, as well as programmable divergence slitting (10 mm radiation length). The measurements were taken with Cu K radiation in the 2 range from 5 to 90° at 40 kV and 40 mA operational conditions; the wavelength was 0.15405 nm. The diffractometer was set up with a sample spinner (Spinner PW3064) and a rotation time of 1 s to get the preferred orientation of crystallites. Predictions for the raw P-XRD patterns were made using High Score (Plus) software and ICDD PDF-4+ 2015.

### Transmission electron microscopy (TEM)

The internal structure of the nanoparticles was studied using transmission electron microscopy (TEM). It was carried out using a Jeol JEM-2100F Field Emission Electron Microscope at an acceleration voltage of 200 kV (JEOL Inc., Akishima, Japan) equipped with a LaB6 power source. The TEM samples were dispersed in methanol, and a drop of the mixture was transferred onto a TEM grid (Cu-grid, 200 mesh) coated with a lacy carbon film.

### Preparation of Au-Fe<sub>3</sub>O<sub>4</sub> nanoparticles

#### Fe<sub>3</sub>O<sub>4</sub> preparations

Chemical co-precipitation method was used for the synthesis of Au-Fe<sub>3</sub>O<sub>4</sub> nanoparticles. This method was selected

because of its simplicity, low production costs, high yield and effectiveness compared to other methods such as microbial incubation which is slow and laborious (Ali et al. 2016). There are two types of co-precipitation methods; the first involves the use of ferrous hydroxides and oxidizing agents. This results in the magnetite (Fe<sub>3</sub>O<sub>4</sub>) with size distribution mean diameter of between 30 and 100 nm. The other involves the stoichiometric mixture of ferrous and ferric salts in aqueous medium to yield magnetic particle of 15–20 nm (Tartaj et al. 2003). The co-precipitation method used was reported by Iancu et al. (2020) and was followed with modifications. A 0.85 mL of conc. HCl (12 M) was diluted with 25 mL ultrapure H<sub>2</sub>O. The prepared solution was used to dissolve 5.2 g of FeCl<sub>3</sub>·6H<sub>2</sub>O (ferric chloride hexahydrate) and 2 g of FeCl<sub>2</sub>·4H<sub>2</sub>O (ferrous chloride tetrahydrate). The Fe<sup>2+</sup>/Fe<sup>3+</sup> ratio was important for the control of morphology and the size of the nanoparticles to be formed (Jolivet et al. 1992). Then, 250 mL of NaOH (1.5 M) was added to the iron mixture. Black precipitate was formed, and it was then separated by an external magnet. The precipitate was washed four times using ultrapure H<sub>2</sub>O. After washing, the back solid was again suspended in 250 mL of ultrapure H<sub>2</sub>O mixed with 1 mL of NaOH (1.5 M). The synthesized Fe<sub>3</sub>O<sub>4</sub>-nanoparticles were stabilized by mixing it with 0.1 M (500  $\mu\text{L}$ ) glucose (Iancu et al. 2020).

#### Au-Fe<sub>3</sub>O<sub>4</sub> preparations

The as-synthesized Fe<sub>3</sub>O<sub>4</sub> NPs were covered with gold (Au) shell by first adding 20 mL of HAuCl<sub>4</sub>·3H<sub>2</sub>O (50 mM) into 105 mL of deionized water followed by boiling. Five millilitres (1 mg/mL) of the as-synthesized Fe<sub>3</sub>O<sub>4</sub> was added into the boiling solution. Sodium citrate (5 mL, 80 mmol/L) was added slowly into the solution under constant stirring. The colour of the solution changed from brown to burgundy. The boiling continued for 5 min. The heat source was removed and stirring continued until the solution cooled to room temperature. Au-Fe<sub>3</sub>O<sub>4</sub> was separated using a permanent magnet (Elbially et al. 2015; Lo et al. 2007; Lu et al. 2006).

#### mSPE of organosulphur compounds for GC-ToFMS analysis

The mSPE procedure was performed by using an appropriate amount of Au-Fe<sub>3</sub>O<sub>4</sub> nanoparticles in a sample glass bottle. A mixture of thiophene, 3-methylthiophene, benzothiophene and dibenzothiophene at 100  $\mu\text{g/g}$  was added and shaken for 10 min to ensure complete pre-concentration of the analyte. The adsorbent and the supernatant were then separated using an external magnet. The supernatant was decanted and 100  $\mu\text{L}$  of eluent (acetonitrile) was introduced to desorb the analyte for 5 min. Figure 1 summarizes the mSPE procedure. 0.22- $\mu\text{m}$  glass membrane/nylon filter was used to filter before injection of 1  $\mu\text{L}$  to a GC-ToFMS for analysis.

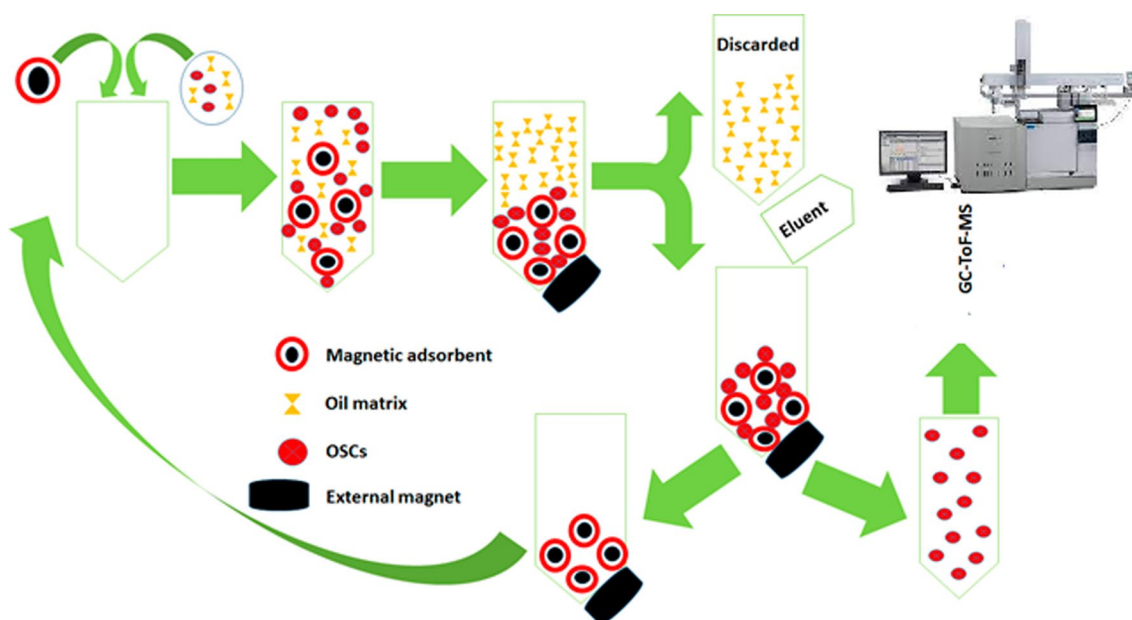


**Fig. 1** Schematic representation of mSPE for the quantitative analysis of OSCs in crude oil samples using GC-ToF-MS

**Table 1** Minimum and maximum amount used for different parameters for screening

| Variable  | Minimum (-) | Maximum (+) |
|---|-------------|-------------|
| Mass of sorbent (mg)                              | 10          | 100         |
| Volume of eluent (acetonitrile) ( $\mu\text{L}$ ) | 100         | 1000        |
| Extraction time (min)                             | 10          | 30          |
| pH  | 4           | 9           |

### Multivariate optimisation

The screening of the most significant variables will be done using the two-level full factorial design ( $2^4$ ) with three replicates. Each factor is studied at two levels coded  $-1$  for low level and  $+1$  for high level. The factorial levels for the four variables are shown in Table 1. The data were assessed using Mini-Tab software which produces a Pareto chart that will indicate significant factors at a certain confidence level based on the red vertical line. The significant figures were further optimized using the response surface methodology. The second-order response surface methodology is based on the central composite design (CCD). The significant parameters from the first-order design are further optimized with the insignificant parameters kept constant. 3D surface plots from Minitab software were used to interpret analytical results (Nomngongo and Ngila 2015). On these plots, the relationship between the response and the parameters is formulated. Furthermore, the effect of each parameter on the extraction

recoveries will be observed (Ndilimeke and Mogolodi 2021).

### Method validation procedure

The m-SPE method was validated by assessing the percentage recovery, the precision in terms of the percentage relative standard deviation, linearity, limit of detection (LOD), limit of quantification (LOQ). A spike recovery strategy was employed for the evaluation of the accuracy at three concentration levels (6, 10 and 25  $\mu\text{g/g}$ ) in triplicate. A six-point calibration curve was used to investigate with standards containing a mixture of target analytes at the concentration 0 to 50  $\mu\text{g/g}$ . Furthermore, the LOD and LOQ were calculated as:

$$\text{LOD} = 3\text{SD}/m \text{ and } \text{LOQ} = 10\text{SD}/m.$$

where SD is the standard deviation of the peak areas and  $m$  is the slope.

The pre-concentration factor was calculated based on the volume of sample ( $v_s$ ) and the volume of the eluent ( $v_e$ ) given by:

$$\text{PF} = v_s/v_e.$$

## Results and discussion

### Characterization of nanoparticles

Surface plasmon resonance (SPR) in gold nanoparticles was intense, resulting in an absorption peak in the visible portion of the electromagnetic spectrum as shown in Fig. 2. This indicated the presence of the gold shell with the superimposed peak of the magnetite without the gold shell. The difference in concentration of the two samples resulted in the intensities to be different also. The surface

plasmon resonance is visible as a peak in Fig. 2 on the visible region, in the range between 520 and 530 nm because of the d–d transition. Elbially et al. (2014); Hien Pham et al. (2008); and Lo et al. (2007) have previously synthesized these nanoparticles and reported the presence of the peak at the same region reported in the current study.

An IR spectrum was used to confirm the identity of functional groups attached to the nanoparticles. The spectra were compared to confirm the functionality. The two spectra in Fig. 3 showed similarities and that indicated that the functionality contained on both nanoparticles is similar in composition with major differences brought about the

**Fig. 2** UV–Vis spectra of  $\text{Fe}_3\text{O}_4$  (red) and  $\text{Au-Fe}_3\text{O}_4$  (black) nanoparticles solution

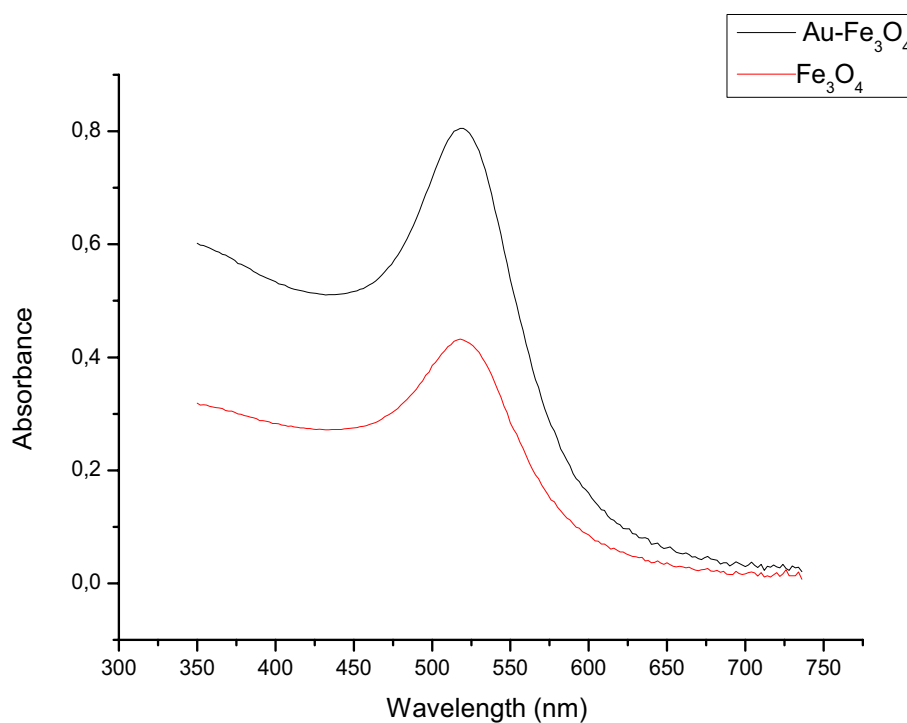
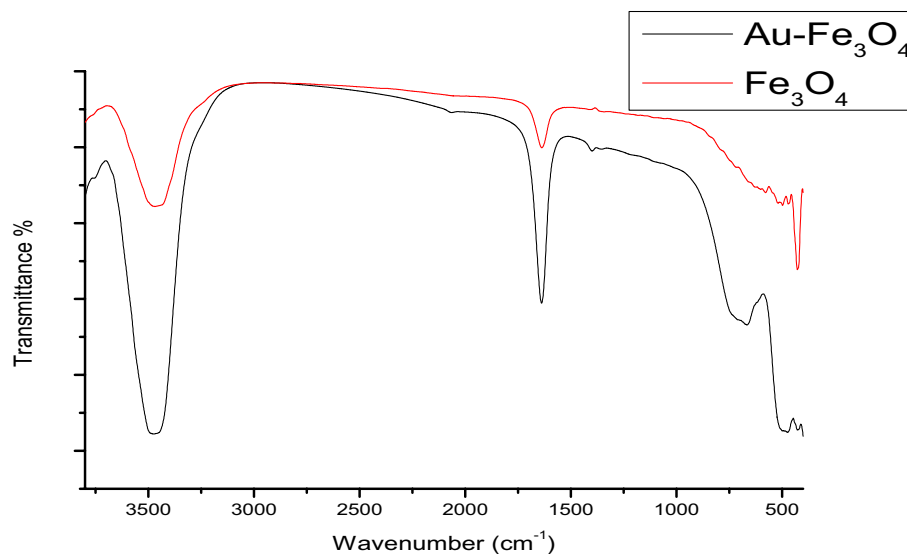


**Fig. 3** FTIR spectrums of  $\text{Fe}_3\text{O}_4$  (red) and  $\text{Au-Fe}_3\text{O}_4$  (black)



peaks at around  $500\text{ cm}^{-1}$ . This peak in  $\text{Fe}_3\text{O}_4$  is brought about the Fe–O stretching vibrational mode of  $\text{Fe}_3\text{O}_4$ . The peak is also present for the Au- $\text{Fe}_3\text{O}_4$  NPs but not sharp and intense because of the presence of Au. Figure 3 shows the peak between  $1500$  and  $1750\text{ cm}^{-1}$  can be assigned to the presence of C=O vibration. The presence of the C=O band can be attributed to citrate used during the synthesis; thus, it can be associated with the –COOH group from the citrate shift. It also indicates the binding of the citrate to the  $\text{Fe}_3\text{O}_4$  nanoparticles. Figure 3 also shows a sharp peak for both IR spectra at  $3492\text{ cm}^{-1}$ . This peak can be assigned to the –OH groups brought about the presence of water on the

surface of the nanoparticles. Stein and co-workers (2020) synthesized and characterized citrate stabilized gold-coated magnetite. During this study, characterization of the nanoparticles using the FTIR showed a Fe–O between  $550$  and  $650\text{ cm}^{-1}$  (Stein et al. 2020) which is in line with what was obtained on current study. In another study, a deprotonated C=O peak was reported at  $1710\text{ cm}^{-1}$  (Ghorbani et al. 2015) which is in agreement with the current synthesis of the gold-coated magnetite.

The nanoparticles are well dispersed and uniform in size as observed by SEM, Fig. 4 A and C. These images show the spherical shapes of both the  $\text{Fe}_3\text{O}_4$  and Au- $\text{Fe}_3\text{O}_4$

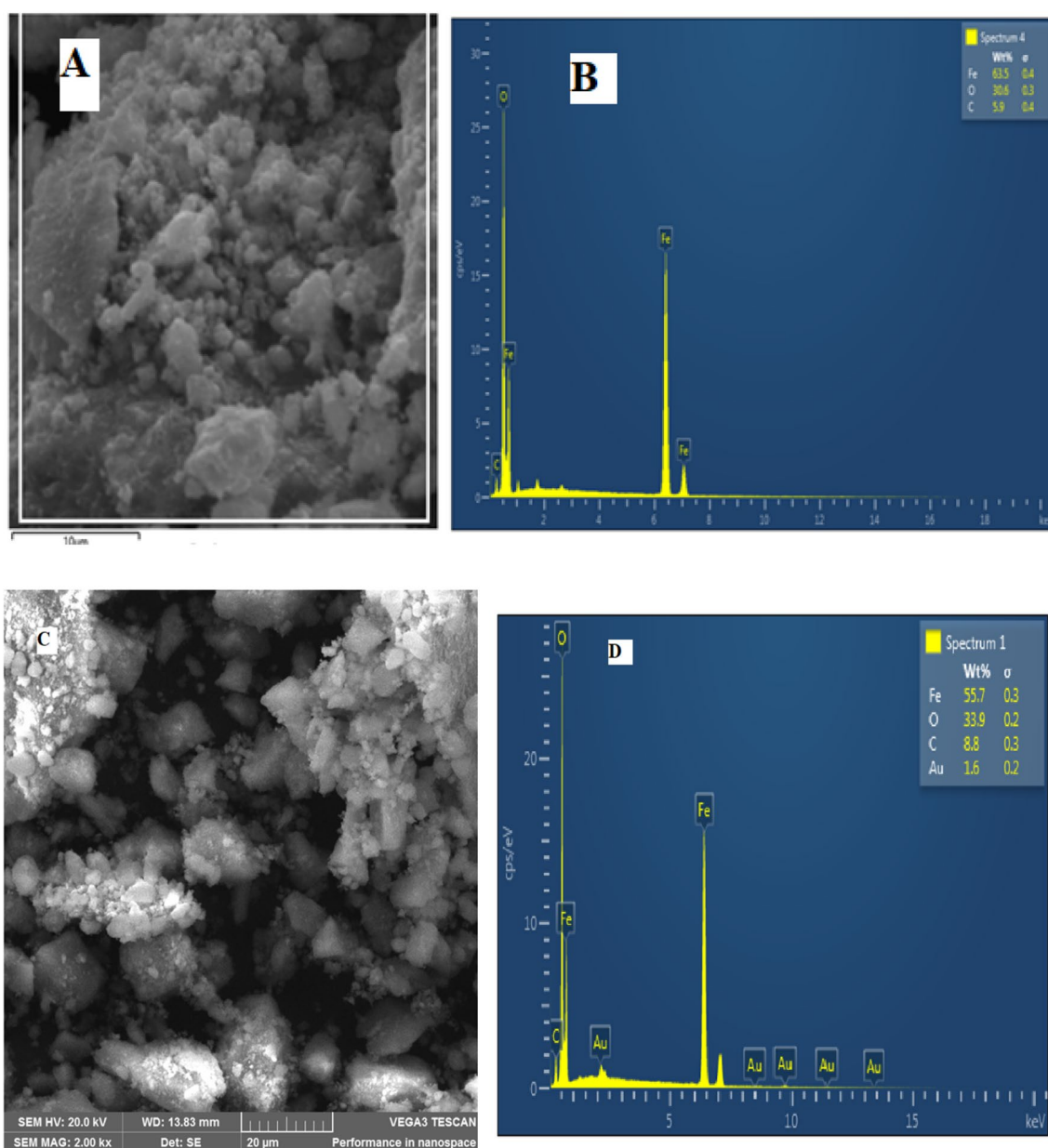


Fig. 4 SEM for A - $\text{Fe}_3\text{O}_4$ , C—Au- $\text{Fe}_3\text{O}_4$ . EDX for B— $\text{Fe}_3\text{O}_4$  and D- Au- $\text{Fe}_3\text{O}_4$

nanoparticles. Furthermore, EDX confirmed that the prepared nanoparticles contained the elements of Fe, C and O (Fig. 4 B) for the synthesized magnetite. The detected signals of carbon arise from the SEM grid. The Au-Fe<sub>3</sub>O<sub>4</sub> nanoparticles are confirmed with Fig. 4 D with elemental distribution of Fe, O, C and Au at 55, 33.9, 8.8 and 1.8 wt. %, respectively, which are elemental composition of Au-Fe<sub>3</sub>O<sub>4</sub>. The presence of Au element is not visible of the non-coated Fe<sub>3</sub>O<sub>4</sub> as expected.

Transmission electron microscope was used to determine the shape and the size of the nanoparticles. The prepared Au-Fe<sub>3</sub>O<sub>4</sub> nanoparticles mostly are spherical in shape, well dispersed and uniform in size as observed by TEM in Fig. 5. The nanoparticles on the image look aggregated which can be due to the magnetic properties it possesses. It also shows a shell in a form of gold that has surrounded the Fe<sub>3</sub>O<sub>4</sub> nanoparticles. Due to the high electronic density of gold when compared to the magnetite, the shell structure of the particles is not visible on TEM, thus the employment of EDX on the previous section. The congruence of TEM with the SEM and EDX is confirmed as explained in the previous section. The Fe<sub>3</sub>O<sub>4</sub> NPs were also spherical in shape with a diameter of about 10 nm. Previous studies of gold-coated magnetite produced similar images (Elbially et al. 2015).

X-ray diffraction patterns of Fe<sub>3</sub>O<sub>4</sub> nanoparticles depict diffraction peaks (Fig. 6) at 30.05, 35.33, 43.01, 53.39, 56.87 and 62.48 $\theta$  which can be indexed to the (220), (311), (400), (422), (511) and (440) planes of Fe<sub>3</sub>O<sub>4</sub> in a cubic phase. The diffraction peaks of Au-Fe<sub>3</sub>O<sub>4</sub> nanoparticles are comparable to those of both Au and Fe<sub>3</sub>O<sub>4</sub> nanoparticles. Their diffraction peaks can be assigned to Au (111), (200), (220), (311) and (222), and Fe<sub>3</sub>O<sub>4</sub> (220), (311), (511) and (440) planes. The penetration of X-rays through the thin gold-coated layer to the central Fe<sub>3</sub>O<sub>4</sub> core can reveal the diffraction peaks for Fe<sub>3</sub>O<sub>4</sub>. The diffraction patterns for both were reported

in the previous studies such as that conducted by Sedki and co-workers (Ivandini et al. 2006).

### Optimization of the extraction procedure

The screening process of most significant factors was conducted using a full factorial design with four independent variables. Mass of the sorbent, pH, eluent volume and time of extraction were chosen as the parameters to be varied. The minimum and maximum amount of each factor was chosen based on the previous studies. Table 1 shows all the factors with the maximum and minimum amount for each factor.

The screening of significant parameters was done using a two-level full factorial design. The analytical response of each OSCs was given in a form of percentage recovery, and the design matrix is displayed in Fig. 7. The design of experiment (DOE) results produced Pareto charts from ANOVA that shows significant parameters on the pre-concentration of OSCs using the magnetic solid phase extraction procedure. The Pareto charts were constructed from four terms combination. The significant parameters are represented by the blue bars shown in Fig. 7 for each individual factor. The red line indicates the 95% confidence level; thus, from Fig. 7 extraction time is the only parameter that passed the 95% confidence level on thiophene, 3-methylthiophene and benzothiophene. Since the other parameters' bar length suggests that they are significant, further optimization is required; thus, the respond surface methodology is employed in the next section. Mass of the sorbent is another parameter which has a long bar length; thus, in the next section, the two parameters, i.e. extraction time and the mass of the sorbent, will be further optimized to improve the recoveries of the OSCs extraction using the mSPE.

Central composite design (CCD) was used for robust mapping during the study to optimize further the parameters that are significant for the pre-concentration of the

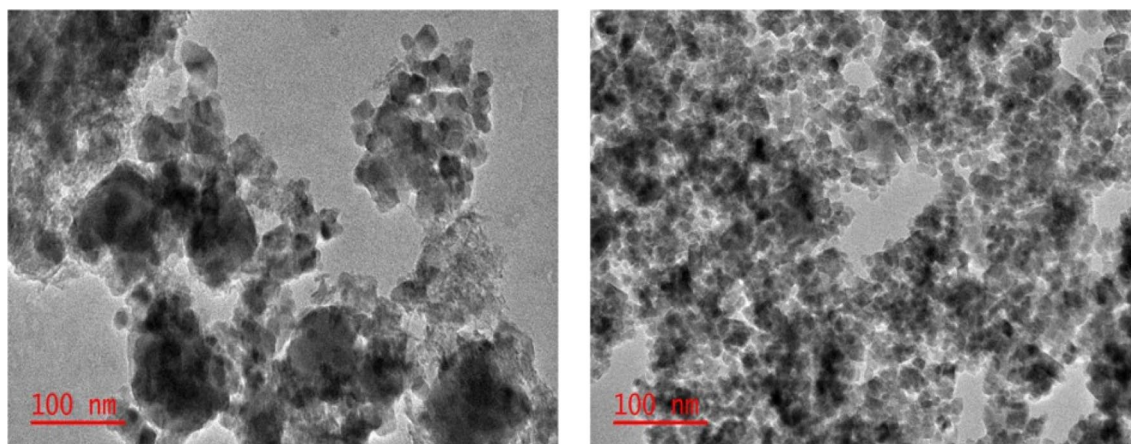
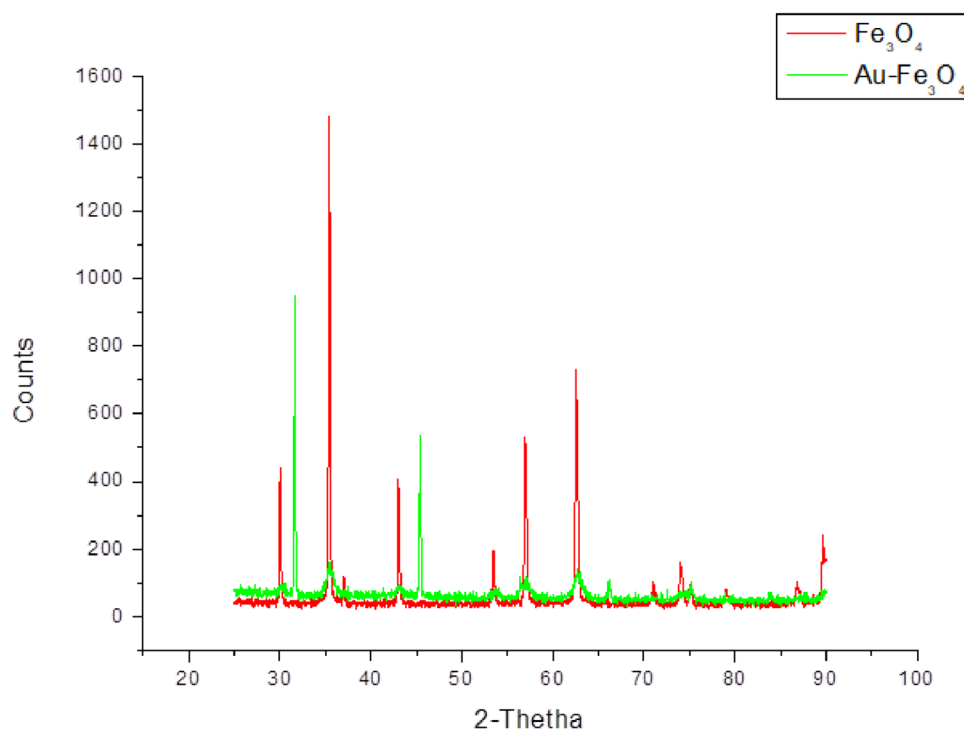


**Fig. 5** Transmission electron microscopy (TEM) images of **A** Fe<sub>3</sub>O<sub>4</sub> and **B** Au-Fe<sub>3</sub>O<sub>4</sub> core shell magnetic nanoparticles

**Fig. 6** P-XRD for  $\text{Fe}_3\text{O}_4$  (red) and  $\text{Au-Fe}_3\text{O}_4$  (green)



OSCs in crude oil samples. Table 2 shows the central composite design matrix and its responses. The CCD deduced the interaction between the parameters under investigation, and it also helped in formulating the quadratic effects of the parameters which are shown in Eqs. 1–4. In this study, two experimental parameters were investigated at a two-level full factorial design with 4 axial points and 5 centre points in cube. The experiments were conducted in triplicate for precision and accuracy. Each run produced 13 base runs with only base block. The central composite designs produced surface plots (Fig. 8A–C) which were produced under optimum conditions to investigate the mass of sorbent (40–120 mg) and the time of extraction (20–60 min). These conditions were informed by the results obtained from the previous section during the screening process. In Fig. 8 it can be clearly seen that recoveries of above 75% for all the OSCs were obtained. For example, Fig. 8C shows that a recovery of more than 90% was obtained with a mass of 100–200 mg and extraction time of around 60 min. The recoveries were satisfactory as they were above 75%. These conditions that yielded this satisfactory recovery were used in the next section for other sample pre-concentration using the magnetic solid phase extraction.

$$\text{Thiophene} = -32,3 + 20,4A + 0,943B - 1,436A^2 - 0,00462B^2 - 0,0142AB \quad (1)$$

$$\begin{aligned} 3\text{-methylthiophene} = & 18,8 + 9,2A + 0,733B - 0,780A^2 \\ & - 0,00515B^2 + 0,0156AB \end{aligned} \quad (2)$$

$$\begin{aligned} \text{Benzothiophene} = & -26,6 + 24,1A + 1,199B - 1,393A^2 \\ & - 0,00247B^2 - 0,1369AB \end{aligned} \quad (3)$$

$$\begin{aligned} \text{Dibenzothiophene} = & -53,2 + 23,1A + 2,050B - 1,44A^2 - 0,00629B^2 - 0,0927AB \end{aligned} \quad (4)$$

### Method validation

The extraction method of OSCs was validated using five concentrations levels of spiked crude oil samples and unspiked samples with three replications for each concentration level. The spike concentration levels for the sample were 6, 10, 17, 22 and 25  $\mu\text{g/g}$  in 100 ml volume. The concentration of the samples was plotted with peak areas to provide information such as the linearity and method calibration. Data summarized in Table 3 show the analytical performance of the instrument for the simultaneous pre-concentration and extraction of the OSCs in crude oil. The correlation factor for this procedure ranged from 0,9816 to 0,9961 for the analysed OSCs. Furthermore, the limit of detection and the limit of quantification ranged from 0,02–0,0416  $\mu\text{g/g}$  to 0,602–0,602  $\mu\text{g/g}$ , respectively. The accuracy of the method was also validated through



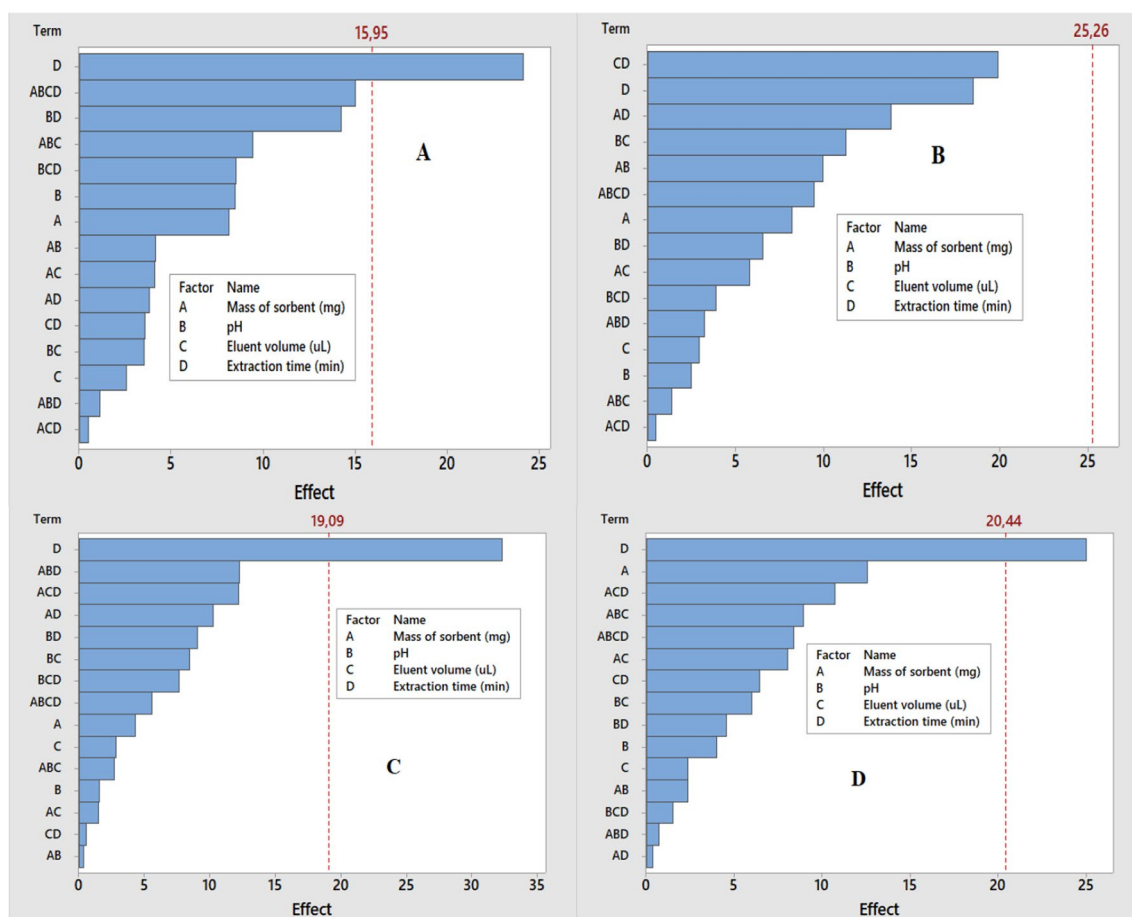


**Fig. 7** Full factorial design Pareto charts ( $n=3$ ) of **A** thiophene, **B** 3-methylthiophene, **C** dibenzothiophene and **D** benzothiophene for the optimization of mass of sorbent, pH, eluent volume and extraction time at 95% confidence level

**Table 2** Respective percentage recoveries of central composite design matrix

| Experiment | Extraction time (min) | Mass of sorbent (mg) | Thiophene | 3-methylthiophene | Benzothiophene | Dibenzothiophene |
|------------|-----------------------|----------------------|-----------|-------------------|----------------|------------------|
| 1          | 40                    | 110                  | 80,3      | 79,3              | 87,9           | 90,1             |
| 2          | 60                    | 200                  | 99,1      | 85,6              | 92,5           | 96,1             |
| 3          | 40                    | 110                  | 68,5      | 73,6              | 77,9           | 81,3             |
| 4          | 20                    | 20                   | 72,1      | 67,2              | 55,4           | 56,3             |
| 5          | 11                    | 110                  | 77,2      | 75,4              | 89,3           | 91,3             |
| 6          | 40                    | 237                  | 61,3      | 56,4              | 89,1           | 66,2             |
| 7          | 68                    | 110                  | 50,2      | 70,8              | 70,1           | 55,5             |
| 8          | 40                    | -17                  | 0         | 0                 | 0              | 0                |
| 9          | 60                    | 20                   | 68,5      | 73,6              | 77,9           | 81,3             |
| 10         | 40                    | 110                  | 70,2      | 67,4              | 69,3           | 70,9             |
| 11         | 20                    | 200                  | 51,4      | 64,2              | 55,6           | 60               |
| 12         | 40                    | 110                  | 71,9      | 77,5              | 81,9           | 90,5             |
| 13         | 40                    | 110                  | 77,9      | 71,9              | 83,9           | 76,5             |

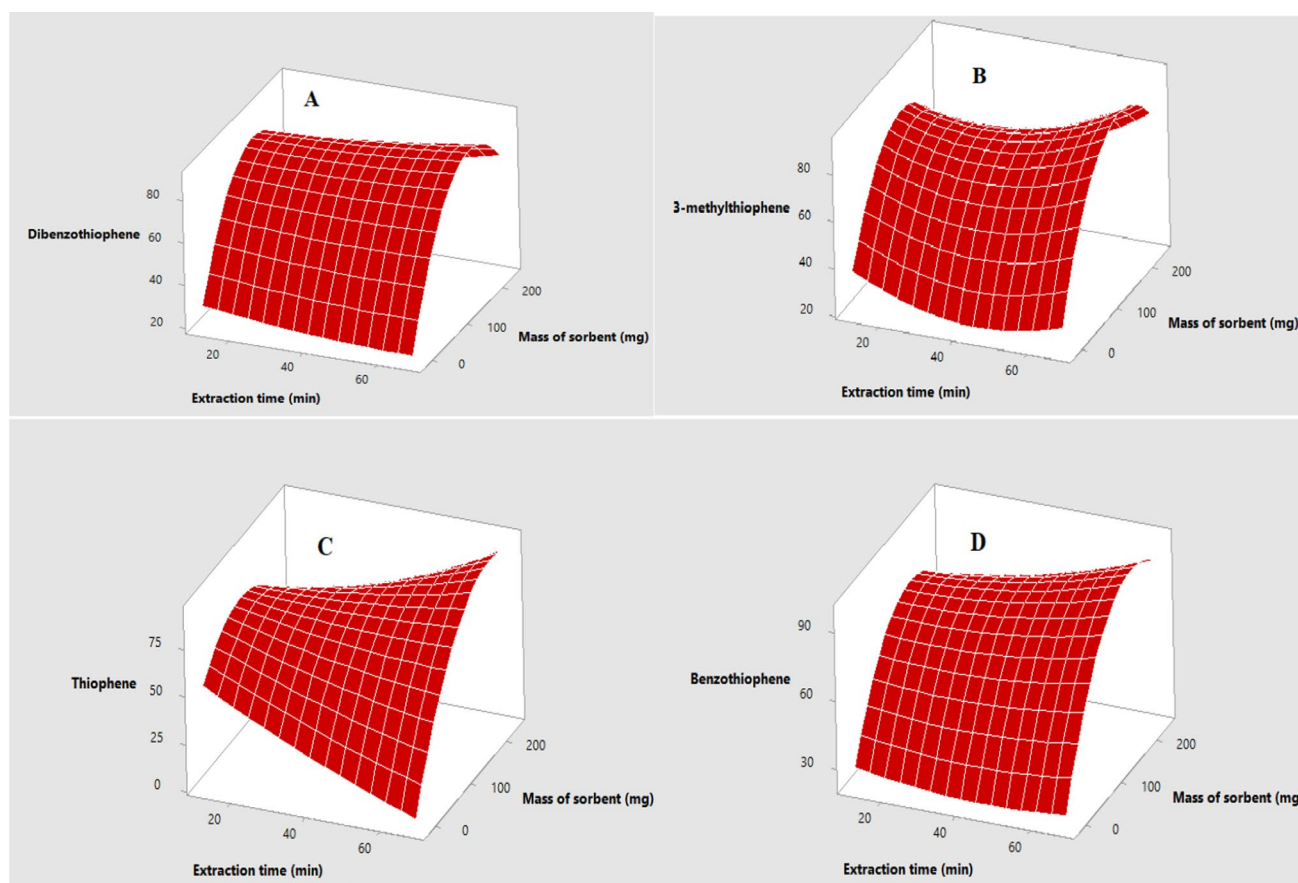


**Fig. 8** Central composite design optimization method for mass of sorbent and extraction time for **A** dibenzothiophene, **B** 3-methylthiophene, **C** thiophene and **D** benzothiophene

**Table 3** Figures of analytical merits for OSCs analysis

| Compound          | LODs ( $\mu\text{g/g}$ ) | LOQs ( $\mu\text{g/g}$ ) | Linearity correlation ( $R^2$ ) | Recovery (%) | Linear Eq. (6–25 $\mu\text{g/g}$ ) | RSD % |
|-------------------|--------------------------|--------------------------|---------------------------------|--------------|------------------------------------|-------|
| Thiophene         | 0,02                     | 0,131                    | 0,9816                          | 76           | $y = 2\text{E}+06x + 2\text{E}+06$ | 1,8   |
| 3-Methylthiophene | 0,0265                   | 0,0806                   | 0,993                           | 93           | $y = 4\text{E}+07x + 8\text{E}+07$ | 1,1   |
| Benzothiophene    | 0,199                    | 0,602                    | 0,9961                          | 88           | $y = 1\text{E}+08x + 7\text{E}+08$ | 0,8   |
| Dibenzothiophene  | 0,0416                   | 0,0126                   | 0,9829                          | 95           | $y = 1\text{E}+08x + 1\text{E}+09$ | 2,3   |

LOD, limit of detection =  $3\text{SD}/m$ ; LOQ limit of quantification =  $10\text{SD}/m$ , relative standard deviation ( $n = 3$ )

the relative standard deviation as it was in the range of 0,9–2,3%. Since the RSD is less than 4%, this indicates that the method relatively has a good precision. The pre-concentration factor was found to be 102.

The use of gold-coated magnetite for pre-concentration of OSCs in real samples can be justified by the chromatogram in Fig. 9, which shows that there is less interference from the complexity of the matrix.

### Comparison with reported literature

Several reports were compiled on different extraction and pre-concentration methods for the OSCs in different samples. The compiled reports are compared with the current study figure of merits. Table 4 gives the summary of the analytical figure of merits of the compiled reports with those of the current study. The linear correlation coefficient was

**Fig. 9** Total ion chromatogram separation of thiophene, 3-methylthiophene, dibenzothiophene and naphtho[2,3]thiophene in crude oil sample

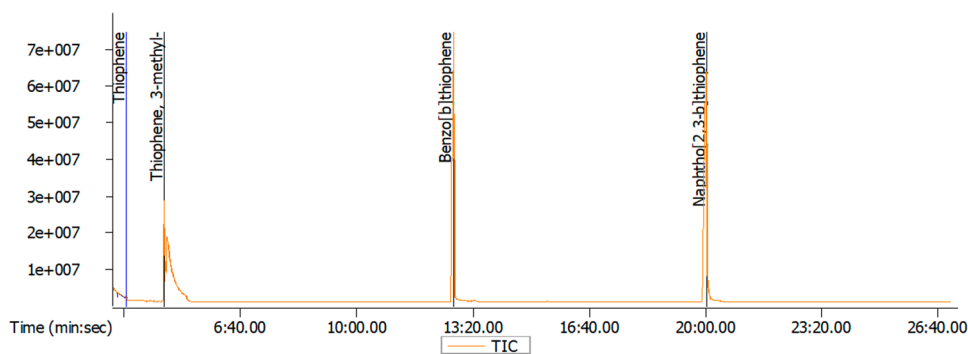


**Table 4** Comparison of analytical merits for developed method with reported literature

| Samples              | OSCs  | Method   | Chromatography | LODs (ppm)   | Correlation R <sup>2</sup> | RSD %      | Refs.                    |
|----------------------|---|----------|----------------|--------------|----------------------------|------------|--------------------------|
| Crude oil and diesel | Benzothiophene, dibenzothiophene and derivatives  | LPME     | GC-SCD         | 0,001–0,111  | 0,98–0,99                  | 4,5–13,8   | Al-Zahrani et al. (2014) |
| Crude oil            | Benzothiophene, dibenzothiophene, and benzo[b]naphtho[1,2-d]thiophene and their derivatives | μ-SPE    | GC-MS          | 0,193–0,597  | 0,9894 to 0,9994           | 3,23–7,52% | Yang et al. (2013)       |
| Coal tar             | Benzo[b]thiophene, Thiophene and its derivatives  | Dilution | GC×GC-ToFMS    | 8,0–30,0     | 0,97,414–0,9882            | 1–4        | Aloisi et al. (2020)     |
| Crude oil            | Thiophene, dibenzothiophene, 3-methylthiophene and benzothiophene                           | m-SPE    | GC-ToF-MS      | 0,02 -0,0199 | 0,9816–0,9961              | 0,8–2,3    | This work                |

found to be 0,9816–0,9961 for the current study which is acceptable for all three spike levels. Furthermore, it has a relatively good precision (0,8–2,3) when compared to other study such as study by Yang et al. (2013). The developed method can be used as an alternative with high precision for the analysis of OSCs. The lowest concentration of the target OSCs that can be quantified was found to be between 0,02 and 0,014 μg/g which is slightly higher when compared to the previous used method. Although the limit of detection is higher, the methods that yield relatively low limit of detection require high extraction time, use of commercially available fibres and low selectivity of the analyte (Ghorbani et al. 2015). Thus, the extraction time of the current study is lower which makes a rapid method and low cost since the adsorbent can be easily synthesized.

### Real sample application

The developed extraction method was then applied on crude oil, diesel, petrol and paraffin sample to detect the amount of OSCs present including the target analytes. This was done using the previously deduced optimum conditions. The amount of these OSCs was detected in some samples as depicted in Table 5. Furthermore, it can clearly be seen that kerosene sample contains the second highest concentration of the OSCs ranging from 1,01 to 3,6 μg/g. Crude oil sample was the highest with concentration of OSCs ranging from 0,13 to 4,09 μg/g. On the other hand, the kerosene sample did not show any presence of a lot of OSCs compounds as compared to the other samples. According to the South African Gazette of March 2021, regulations for fuel should be less than 10 ppm (DoE 2014) for total sulphur which is the sum of OSCs per sample. During the analysis of the

**Table 5** Concentration of OSCs in crude oil, diesel, gasoline and kerosene samples using mSPE

| Organosulphur compounds                                     | Crude oil ( $\mu\text{g/g}$ ) | Diesel ( $\mu\text{g/g}$ ) | Gasoline ( $\mu\text{g/g}$ ) | Kerosene( $\mu\text{g/g}$ ) |
|---|-------------------------------|----------------------------|------------------------------|-----------------------------|
| Acetic acid, mercapto-                                      | $0,3 \pm 0,005$               | $0,02 \pm 0,001$           | $1,06 \pm 0,007$             | ND                          |
| Disulfide, diphenyl   | ND                            | $0,1 \pm 0,02$             | $3,06 \pm 0,02$              | ND                          |
| Benzo[b]naphtho[2,3-d]thiophene, 9,10-dihydro-6,7-dimethyl- | $1,06 \pm 0,004$              | $0,012 \pm 0,1$            | $3,05 \pm 0,04$              | $1,01 \pm 0,05$             |
| Disulfide, bis(4-methylphenyl)                              | ND                            | $0,41 \pm 0,06$            | ND                           | $5,02 \pm 0,0001$           |
| Benzothiophene  | $0,98 \pm 0,1$                | $1,02 \pm 0,08$            | $4,31 \pm 0,09$              | $2,1 \pm 0,009$             |
| Benzene methanethiol, TMS derivative                        | $0,13 \pm 0,08$               | ND                         | $0,46 \pm 0,003$             | $3,6 \pm 0,2$               |
| 2-Thiophenecarboxylic acid, 5-tert-butyl-                   | $1,02 \pm 0,05$               | $3,06 \pm 0,03$            | $2,06 \pm 0,01$              | $1,9 \pm 0,003$             |
| Thiophene   | $1,94 \pm 0,05$               | $1,65 \pm 0,02$            | $0,43 \pm 0,01$              | $1,53 \pm 0,06$             |
| Acetic acid, mercapto-                                      | $1,93 \pm 0,03$               | ND                         | ND                           | ND                          |
| 3-methylthiophene   | $0,9 \pm 0,02$                | $1,63 \pm 0,11$            | $0,98 \pm 0,04$              | $0,78 \pm 0,03$             |
| Benzo[b]thiophene, 3-phenyl-                                | $0,35 \pm 0,02$               | $2,15 \pm 0,009$           | ND                           | $2,45 \pm 0,004$            |
| Thiophene, 2-iodo-  | $2,05 \pm 0,07$               | ND                         | $1,04 \pm 0,005$             | ND                          |
| 5-Bromo-2-thiophenecarboxaldehyde                           | $4,09 \pm 0,1$                | $2,01 \pm 0,003$           | $2,65 \pm 0,03$              | $1,43 \pm 0,4$              |
| Dibenzothiophene  | $1,55 \pm 0,08$               | $1,64 \pm 0,01$            | $2,09 \pm 0,09$              | $1,19 \pm 0,01$             |
| Thioxanthene  | ND                            | $0,9 \pm 0,006$            | $1,12 \pm 0,05$              | ND                          |

Experimental conditions: volume of eluent, 100  $\mu\text{L}$ ; mass of sorbent, 150 mg; time of extraction, 50 min; and pH of sample, 6,7

samples, other OSCs compounds such a which were not a target during the study were visible.

## Conclusion

The quantitative analysis of crude oil, diesel, gasoline and kerosene was performed using the mSPE procedure for sample pre-treatment and pre-concentration of the OSCs prior to analysis. During the employment of this method, a magnetic sorbent in a form of gold-coated magnetite nanoparticles was synthesized. The synthesized nanoparticles were successfully characterized to confirm the formation of the Au-Fe<sub>3</sub>O<sub>4</sub> nanoparticles. It was used as an adsorbent with four factors being considered for optimization. These were: the volume of the eluent (100–1000  $\mu\text{L}$ ), the pH of the sample (4–9), the extraction time (10–30 min) and the mass of the adsorbent (10–100 mg). Using the full factorial design, screening of the most significant parameters was done. Through Pareto charts produced from the full factorial design based on the four parameters, it was found that extraction time and mass of adsorbent were found to be the most significant parameters. These significant figures were further optimized using the central composite design (CCD) as the response surface methodology to find the optimum conditions. The optimum condition was found to be 150 mg for the mass of sorbent and 50 min for the time of extraction. The other conditions that were kept constant are eluent volume which was 100  $\mu\text{L}$  and the pH of the sample was kept at 6.7.

Coupling the GC-ToFMS with the developed sample pre-treatment method yielded an improved correlation

factor of 0,9816–0,9961, better sensitivity of 0,8–2,3% and acceptable recoveries of 76–95%. The limit of quantification and the limit of detection were found to be in the range of 0,08–0,602  $\mu\text{g/g}$  and 0,02–0,199  $\mu\text{g/g}$ , respectively. Upon analysing the concentration of OSCs in crude oil, gasoline, diesel and kerosene it was found to be in ranged of 0,3–4,09  $\mu\text{g/g}$ , 1,06–1,65  $\mu\text{g/g}$ , 0,02–3,06  $\mu\text{g/g}$  and 1,01–5,02  $\mu\text{g/g}$ , respectively. The concentration of OSCs on these samples was in acceptable level according to the South African Petroleum regulations. The developed method can be used as an alternative method for sample pre-treatment. This method was rapid and less costly when compared with the previously employed method.

**Acknowledgements** The authors would like to thank South African National Research Foundation-THUTHUKA (113951), University of South Africa, for their financial support.

**Funding** Open access funding provided by University of South Africa.

**Data availability** All data generated or analysed during this study are included in this published article and its supplementary information file.

## Declarations

**Conflict of interest** The authors declare no conflict of interest of any form.

**Open Access** This article is licensed under a Creative Commons Attribution 4.0 International License, which permits use, sharing, adaptation, distribution and reproduction in any medium or format, as long as you give appropriate credit to the original author(s) and the source, provide a link to the Creative Commons licence, and indicate if changes were made. The images or other third party material in this article are

included in the article's Creative Commons licence, unless indicated otherwise in a credit line to the material. If material is not included in the article's Creative Commons licence and your intended use is not permitted by statutory regulation or exceeds the permitted use, you will need to obtain permission directly from the copyright holder. To view a copy of this licence, visit <http://creativecommons.org/licenses/by/4.0/>.

## References

- Ali A, Zafar H, Zia M, ul Haq I, Phull AR, Ali JS, Hussain A (2016) Synthesis, characterization, applications, and challenges of iron oxide nanoparticles. *Nanotech, Sci Appl* 9:49–67. <https://doi.org/10.2147/NSA.S99986>
- Aloisi I, Zoccali M, Tranchida PQ, Mondello L (2020) Analysis of organic sulphur compounds in coal tar by using comprehensive two-dimensional gas chromatography-high resolution time-of-flight mass spectrometry. *Separations* 7(2):3–11. <https://doi.org/10.3390/separations7020026>
- Al-Zahrani I, Basheer C, Htun T (2014) Application of liquid-phase microextraction for the determination of sulfur compounds in crude oil and diesel. *J Chromatogr A* 1330:97–102. <https://doi.org/10.1016/j.chroma.2014.01.015>
- Andersson JT, Hegazi AH, Roberz B (2006) Polycyclic aromatic sulfur heterocycles as information carriers in environmental studies. *Anal Bioanal Chem* 386(4):891–905. <https://doi.org/10.1007/s00216-006-0704-y>
- Biehl P, Schacher FH (2020) Surface functionalization of magnetic nanoparticles using a thiol-based grafting-through approach. *Surfaces* 3(1):116–131. <https://doi.org/10.3390/surfaces3010011>
- da Silveira GD, Hoinacki CK, Bueno Goularte R, Do Nascimento PC, Bohrer D, Cravo M, Leite LFM, de Carvalho LM (2017) A cleanup method using solid phase extraction for the determination of organosulfur compounds in petroleum asphalt cements. *Fuel* 202:206–215. <https://doi.org/10.1016/j.fuel.2017.04.020>
- DoE. (2014). Government Gazette Staatskoerant. Government Gazette, 583(37230), 1–4. [http://www.greengazette.co.za/pages/national-gazette-37230-of-17-january-2014-vol-583\\_20140117-GGN-37230-003](http://www.greengazette.co.za/pages/national-gazette-37230-of-17-january-2014-vol-583_20140117-GGN-37230-003)
- Elbially NS, Fathy MM, Khalil WM (2014) Preparation and characterization of magnetic gold nanoparticles to be used as doxorubicin nanocarriers. *Physica Med* 30(7):843–848. <https://doi.org/10.1016/j.ejmp.2014.05.012>
- Elbially NS, Fathy MM, Khalil WM (2015) Doxorubicin loaded magnetic gold nanoparticles for in vivo targeted drug delivery. *Int J Pharm* 490(1–2):190–199. <https://doi.org/10.1016/j.ijpharm.2015.05.032>
- Garcia KO, Frena M, Bittencourt OR, Magosso HA, Carasek E, Madureira LAS (2021) A green procedure using disposable pipette extraction to determine polycyclic aromatic sulfur heterocycles in water samples and solid petrochemical residues. *J Braz Chem Soc* 32(2):277–286. <https://doi.org/10.21577/0103-5053.20200178>
- Ghorbani M, Hamishehkar H, Arsalani N, Entezami AA (2015) Preparation of thermo and pH-responsive polymer@Au/Fe<sub>3</sub>O<sub>4</sub> core/shell nanoparticles as a carrier for delivery of anticancer agent. *J Nanopart Res* 17(7):1–13. <https://doi.org/10.1007/s11051-015-3097-z>
- Heidari H, Razmi H (2012) Multi-response optimization of magnetic solid phase extraction based on carbon coated Fe<sub>3</sub>O<sub>4</sub> nanoparticles using desirability function approach for the determination of the organophosphorus pesticides in aquatic samples by HPLC-UV. *Talanta* 99:13–21. <https://doi.org/10.1016/j.talanta.2012.04.023>
- Hien Pham TT, Cao C, Sim SJ (2008) Application of citrate-stabilized gold-coated ferric oxide composite nanoparticles for biological separations. *J Magn Magn Mater* 320(15):2049–2055. <https://doi.org/10.1016/j.jmmm.2008.03.015>
- Hill PG, Smith RM (2000) Determination of sulphur compounds in beer using headspace solid-phase microextraction and gas chromatographic analysis with pulsed flame photometric detection. *J Chromatogr A* 872(1–2):203–213. [https://doi.org/10.1016/S0021-9673\(99\)01307-2](https://doi.org/10.1016/S0021-9673(99)01307-2)
- Iancu SD, Albu C, Chiriac L, Moldovan R, Stefanu A, Moisoiu V, Coman V, Szabo L, Leopold N, Bálint Z (2020) Assessment of gold-coated iron oxide nanoparticles as negative T2 contrast agent in small animal MRI studies. *Int J Nanomed* 15:4811–4824. <https://doi.org/10.2147/IJN.S253184>
- Ivandini TA, Sato R, Makide Y, Fujishima A, Einaga Y (2006) Electrochemical detection of arsenic (III) using electrodes. *Anal Chem* 78(18):6291–6298
- Jolivet JP, Belleville P, Tronc E, Livage J (1992) Influence of Fe(II) on the formation of the spinel iron oxide in alkaline medium. *Clays Clay Miner* 40(5):531–539. <https://doi.org/10.1346/CCMN.1992.0400506>
- Khalilian F, Rezaee M (2014) Extraction and determination of organosulfur compounds in water samples by using homogeneous liquid-liquid microextraction via flotation assistance-gas chromatography-flame ionization detection. *Bull Chem Soc Ethiop* 28(2):195–204. <https://doi.org/10.4314/bcse.v28i2.4>
- Lau ECHT, Åhlén M, Cheung O, Ganin AY, Smith DGE, Yiu HHP (2023) Gold-iron oxide (Au/Fe<sub>3</sub>O<sub>4</sub>) magnetic nanoparticles as the nanopatform for binding of bioactive molecules through self-assembly. *Front Mol Biosci* 10(March):1–8. <https://doi.org/10.3389/fmolb.2023.1143190>
- Liu P, Shi Q, Chung KH, Zhang Y, Pan N, Zhao S, Xu C (2010) Molecular characterization of sulfur compounds in venezuela crude oil and its SARA fractions by electrospray ionization fourier transform ion cyclotron resonance mass spectrometry. *Energy Fuels* 24(9):5089–5096. <https://doi.org/10.1021/ef100904k>
- Lo CK, Xiao D, Choi MMF (2007) Homocysteine-protected gold-coated magnetic nanoparticles: synthesis and characterisation. *J Mater Chem* 17(23):2418–2427. <https://doi.org/10.1039/b617500g>
- Lu QH, Yao KL, Xi D, Liu ZL, Luo XP, Ning Q (2006) Synthesis and characterization of composite nanoparticles comprised of gold shell and magnetic core/cores. *J Magn Magn Mater* 301:44–49. <https://doi.org/10.1016/j.jmmm.2005.06.007>
- Manousi N, Deliyanni EA, Rosenberg E, Zachariadis GA (2021) Magnetic solid-phase extraction of caffeine from surface water samples with a micro-meso porous activated carbon/Fe<sub>3</sub>O<sub>4</sub>-nanocomposite prior to its determination by GC-MS. *RSC Adv* 11(32):19492–19499. <https://doi.org/10.1039/d1ra01564h>
- Mgiba SS, Mhuka V, Mketi N (2021) Trends in the direct and indirect chromatographic determination of organosulfur compounds in various matrices trends in the direct and indirect chromatographic determination of organosulfur compounds in various matrices. *Sep Purif Rev* 00(00):1–13. <https://doi.org/10.1080/15422119.2020.1866011>
- Ndilimeke M, Mogolodi K (2021) Ultrasonic assisted magnetic solid phase extraction based on the use of magnetic waste-tyre derived activated carbon modified with methyltriocylammonium chloride adsorbent for the preconcentration and analysis of non-steroidal anti-inflammatory drugs in. *Arab J Chem* 14(9):103329. <https://doi.org/10.1016/j.arabjc.2021.103329>
- Nomngongo PN, Ngila JC (2015) Multivariate optimization of dual-solid phase extraction for preconcentration of Ag, Al, As and Cr in gasoline prior to inductively coupled plasma optical emission spectrometric determination. *Fuel* 139:285–291. <https://doi.org/10.1016/j.fuel.2014.08.046>

- Patel K, Panchal N, Ingle P (2019) Review of extraction techniques extraction methods: microwave, ultrasonic, pressurized fluid, Soxhlet extraction, etc. *Int J Adv Res Chem Sci* 6(3):6–21
- Stein R, Friedrich B, Mühlberger M, Cebulla N, Schreiber E, Tietze R, Cicha I, Alexiou C, Dutz S, Boccaccini AR, Unterwiesing H (2020) Synthesis and characterization of citrate-stabilized gold-coated superparamagnetic iron oxide nanoparticles for biomedical applications. *Molecules* 25(19):4425. <https://doi.org/10.3390/molecules25194425>
- Šulek F, Drofenik M, Habulin M, Knez Ž (2010) Surface functionalization of silica-coated magnetic nanoparticles for covalent attachment of cholesterol oxidase. *J Magn Magn Mater* 322(2):179–185. <https://doi.org/10.1016/j.jmmm.2009.07.075>
- Tan L, Zhang X, Liu Q, Jing X, Liu J, Song D, Hu S, Liu L, Wang J (2015) Synthesis of Fe<sub>3</sub>O<sub>4</sub>/TiO<sub>2</sub> core-shell magnetic composites for highly efficient sorption of uranium (VI). *Colloids Surf, A* 469:279–286. <https://doi.org/10.1016/j.colsurfa.2015.01.040>
- Tartaj P, Morales MP, Veintemillas-Verdaguer S, González-Carreño T, Serna CJ (2003) Preparation of magnetic nanoparticles for applications in biomedicine. *J Phys D: Appl Phys* 36(13):52–67. <https://doi.org/10.1088/0022-3727/36/13/202>
- Yang B, Hou W, Zhang K, Wang X (2013) Application of solid-phase microextraction to the determination of polycyclic aromatic sulfur heterocycles in Bohai Sea crude oils. *J Sep Sci* 36(16):2646–2655. <https://doi.org/10.1002/jssc.201300184>
- Yu C, Li X, Hu B (2008) Preparation of sol-gel polyethylene glycol-polydimethylsiloxane-poly(vinyl alcohol)-coated sorptive bar for the determination of organic sulfur compounds in water. *J Chromatogr A* 1202(1):102–106. <https://doi.org/10.1016/j.chroma.2008.06.012>
- Zhao L, Gao M, Yue W, Jiang Y, Wang Y, Ren Y, Hu F (2015) Sandwich-structured graphene-Fe<sub>3</sub>O<sub>4</sub>@carbon nanocomposites for high-performance lithium-ion batteries. *ACS Appl Mater Interfaces* 7(18):9709–9715. <https://doi.org/10.1021/acsami.5b01503>

**Publisher's Note** Springer Nature remains neutral with regard to jurisdictional claims in published maps and institutional affiliations.